IJCRT.ORG ISSN : 2320-2882

INTERNATIONAL JOURNAL OF CREATIVE RESEARCH THOUGHTS (IJCRT)

An International Open Access, Peer-reviewed, Refereed Journal

Design And Simulation Of Magnetically Responsive Cementitious Composites Towards Efficient Crack Closure In Road Construction

[1]Rajat, [2]Er. Rajbala*

[1]M. Tech. Scholar, [2]Asst. Professor

[1, 2,] Department of Civil Engineering

[1 , 2,]Affiliation Address: Jan Jayak Chaudhary Devi Lal Memorial College of Engineering, Sirsa, Haryana, India

Abstract

The deterioration of road infrastructure due to cracking and environmental stress demands advanced self-healing solutions beyond conventional repairs. This study presents the development of Magnetically Responsive Cementitious Composites (MRCC) for efficient crack closure in road construction. MRCC integrates magnetic particles and Shape Memory Polymer (SMP) fibers, enabling remote, targeted, and autonomous crack repair through magnetic or thermal activation. Knotted SMP (k-SMP) fibers made from polyethylene terephthalate (PET) were embedded in mortar with aligned (AD) and random (RD) distributions. Experimental tests included three-point bending, optical crack width measurement, and thermal activation at 150°C to trigger fiber shrinkage. Results showed significant crack reduction, with AD specimens achieving up to 77% closure and some complete healing, while RD specimens averaged 45% closure. X-ray computed tomography confirmed the critical role of fiber alignment in enhancing self-healing performance. This research demonstrates MRCC's potential for smart, durable, and low-maintenance road infrastructure.

Keywords: Crack closure, MRCC, Knotted SMP, Construction.

1. Introduction

The rapid deterioration of road infrastructure through cracking, fatigue, and environmental causes is a major threat to the world's transportation networks [1,2]. Road pavement cracks not only weaken structural integrity but also speed up the deterioration process, which leads to expensive repairs, higher maintenance requirements, and possible safety risks for traffic users [3,4]. Conventional practices of road maintenance and repair are frequently reactive, time and resource-intensive, and costly, particularly for areas with large transport networks and few resources [5]. In response to such limitations, there is growing interest in creating new self-healing materials that have the ability to repair cracks by themselves and restore the performance of road surfaces, extending the latter's lifespan and improving overall infrastructure robustness [6]. Among different self-healing materials, Magnetically Responsive Cementitious Composites (MRCCs) are seen to be a promising candidate for effective and localized crack closure in road construction applications [7,8].

MRCCs consist of magnetic particles including iron oxide or ferrite-based media being embedded into normal cementitious media [9]. Activation of these magnetic fillers in the matrix provides the composite with special features so that the latter can react according to an external magnetic field. These composites will either display the ability to align particles, locally heat (through induction) or induce a controlled motion of the embedded materials when an applied magnetics stimulus is applied which can also allow crack closing and healing to take place within the cement matrix [10]. The given approach carries greater benefits compared to the passive self-healing techniques, since it can be remotely triggered, localised to specific repair areas within the damaged areas only, and it can be implemented to improve the mechanical performance of a structure, without the need to alter the structural design. In the context of road construction, MRCCs present an attractive alternative to conventional materials, providing a pathway for smarter, more durable, and cost-effective pavements capable of mitigating crack propagation at an early stage [11].

Figure 1: Multiple types of road pavement failures [12].

MRCCs should be designed and simulated using the integrated approach to road building (material science, structural engineering, computation modelling) [13]. The right choice of magnetic fillers, their existence best spreads within the cementitious ground, and the knowledge regarding how they interact with external magnetic fields are the key aspects that can attest to the efficiency of the crack closing mechanism [14,15]. In addition, the rheological characteristics, strength, durability and suitability to the environment of the composite should be analyzed systematically so that it can be suitable to be practical in terms of being used in road building.

In this work, the structuring, design, and simulation of magnetically (MRCC) responsive cementitious composites for practical use in effective crack closure in road construction is emphasized. The goal of the research is to assess the role of magnetic filler amount, distribution methodology, and magnetic activation methods on the mechanical performance and self-healing efficiency of a composite. Using computational modeling and simulation, this paper provides a a more thorough framework for optimizing MRCCs, and will help pave the way for the future use of smart, self-healing materials for roads designed to improve the durability and sustainability of transportation infrastructure. Here are the researches objectives of the study are following as:

- To design and develop MRCC by incorporating magnetic fillers to enhance the self-healing efficiency and crack closure potential of road construction materials.
- To experimentally evaluate the crack-closing performance of knotted Shape Memory Polymer (k-SMP) fibers embedded in mortar, considering different fiber distributions (aligned and random) and the effect of thermal activation.
- To utilize computational modeling and X-ray computed tomography (X-CT) to analyze the internal orientation of fibers, crack bridging behavior, and overall efficiency of the MRCC system for self-healing under simulated road conditions.
- To compare the effectiveness of MRCC in reducing crack widths below critical thresholds for autogenous repair, thereby enhancing the durability, resilience, and service life of transportation infrastructure.

2. Methods and Materials

2.1 Material Used

- **Mortar paste**

It was made using regular water, average quartz sand for the fine aggregate, and conventional Portland cement "CEM II A/L 32.5 R". The mass ratio of cement to sand was 1:3, while for water to cement was 0.5. The sand, cement, and water mixture parameters were 485.3 kg/m^3, 1521.4 kg/m^3, and 251.5 kg/m^3, correspondingly.

- **k-SMP Fibres**

This work made use of shape memory polymer (SMP) fibers that were produced at the University of Bradford in the United Kingdom using granular Dow Lighter C93 commercial grade "polyethylene terephthalate (PET)". To accomplish molecular orientation in the fibers, melt extrusion was used to create the fibers, and then die drawing was used [16,17]. The "stress-strain curves" for 3 filament samples, which are nominally comparable, are shown in Figure 2. These samples are filaments A,B,C.

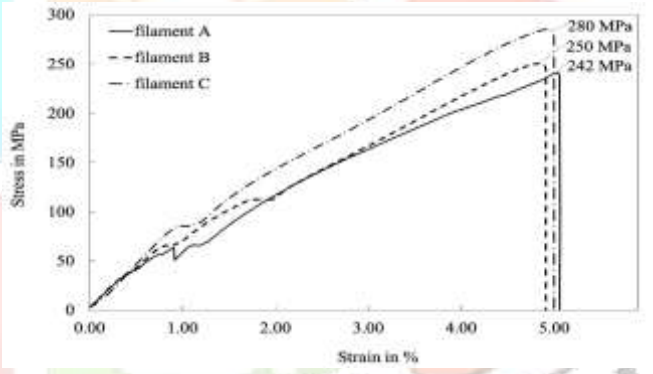

Figure 2: Tensile behavior of SMP filaments

The filaments exhibited a median strain at failure of 6% and a stress at failure of around 257 MPa (CV = 9%). In the first scenario, an only filament measuring 200±1 mm was held in a warmed chamber. As the temperature was raised to specific targets of 90, 100, and 150 ◦C, the stress resulting from the controlled shrinkage was recorded. Specimens were warmed to optimum temperatures of 100 and 90 ◦C, resulting in peak stresses of 42 and 40MPa, respectively, while the filament was warmed to an ideal temperature of 150 ◦C, yielding a peak stress measurement of 51MPa. Figure 3 reports the measurements in detail.

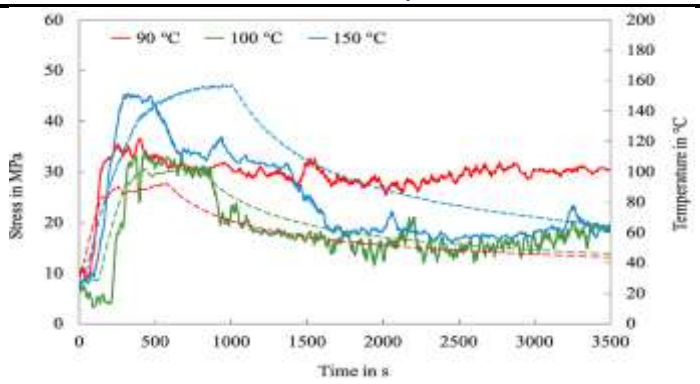

Figure 3: Developing controlled shrinkage stresses in warmed SMP filaments at 90, 100, and 150℃

Filaments with an actual length of 100 ±1 mm ($L_{f,eff}$) were used to quantify free shrinkage. The filaments were put in a preheated oven and left there for 10, 20, and 30 minutes at 100, 120, and 150 ◦C, respectively. Figure 4a displays the average shrinkage (in %) for fibers with straight ends and Figure 4b displays the same data for knotted ends.

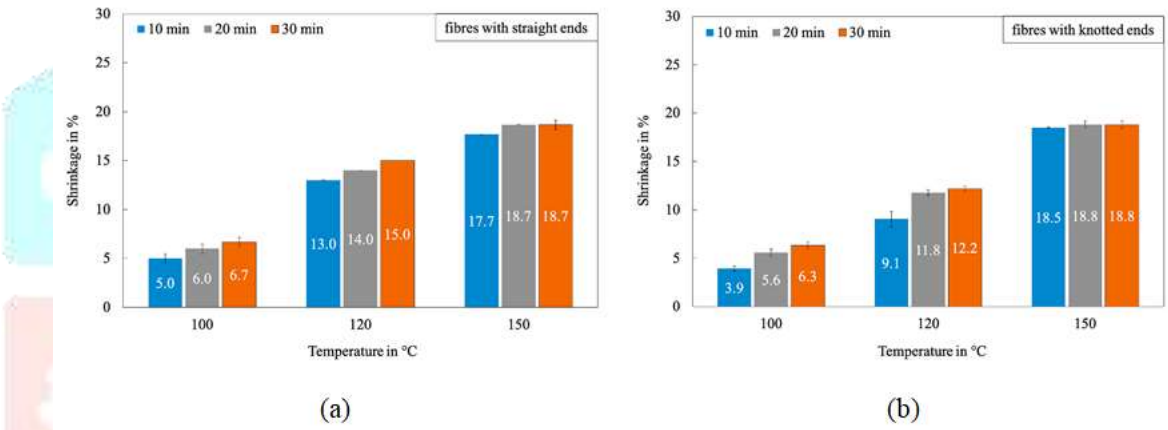

Figure 4: Potential for free shrinkage of (a) fibers include untwisted ends and (b) fibers include knotted ends subjected to varying heating times and target temperatures

The ends of the individual fibers were placed in mortar cubes of 25 × 25 × 25 mm in such a way that the embedment length at each end of the fibers was 20 ±1 mm, as seen in Figure 5a and Figure 5b. The fiber ends were then encased in cubes and let to cure at room temperature for a week. As seen in Figure 5c, the cubes were encased in steel plates.

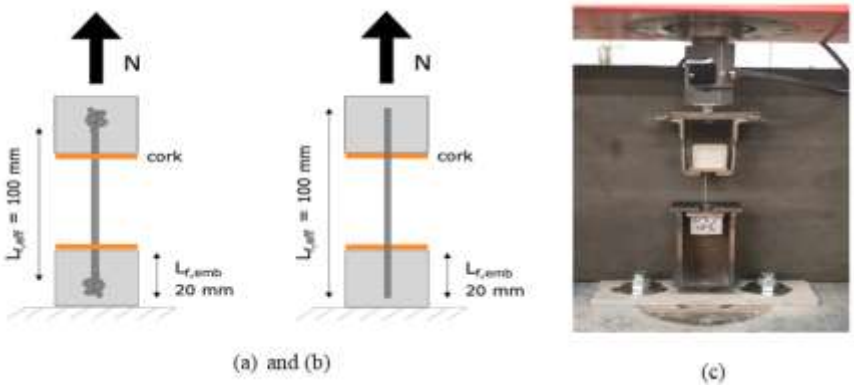

Figure 5: Establishment for testing the mechanical anchorage's resilience (a) Fibers formed by knotted strands b) Fibers that are straight (c) The sample is inserted into the testing equipment

Complete pull-out occurred in the straight-ended samples subjected to loads ranging from 10 to 30 N (Figure 6). Figure 6 shows that the knotted fibers could endure loads between 230 and 290 N, which are much greater than the normal limits.

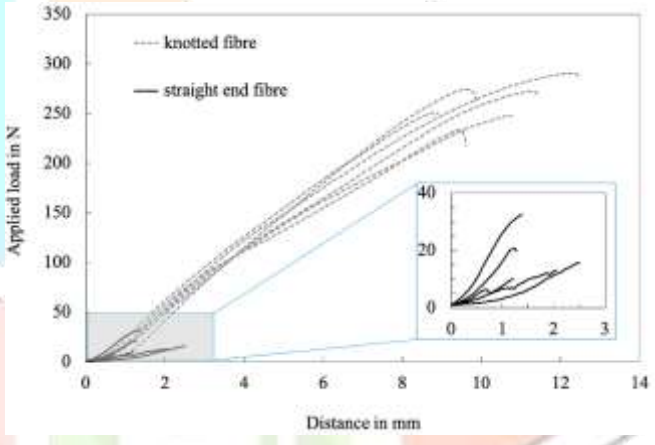

Figure 6: Analysis of knotted and straight-end fiber anchorage resistance curves

2.2 Methods for preparing specimens for testing

A conventional bowl mixer and processes in accordance with BS EN 196-1:2016 were used to create the mortar paste. Two distinct molds were used for casting mortar beams: one small (160 × 40 × 40 mm) and one big (250 × 75 × 75 mm). Small beams with aligned fibers (AD) and big beams with a random distribution and orientation of fibers (RD) were the two specimen designs used, as shown in Figure 7.

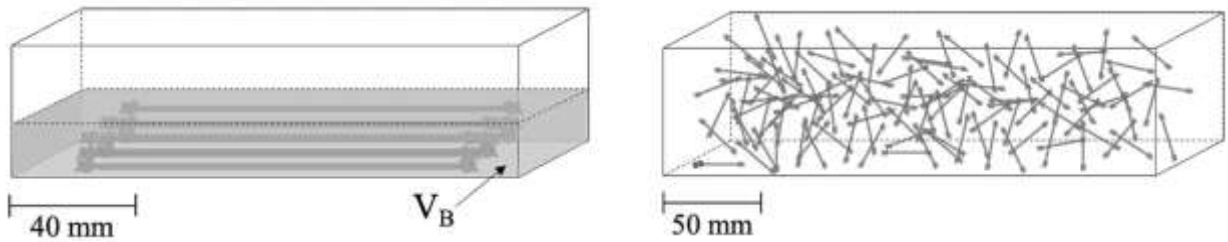

Figure 7: Illustration of specimens in a schematic format

2.3 Estimation of Crack Openings

To ensure accurate strength measurements, entirely specimens were oven-dried at 50℃ for 24 hours after curing for 28 days. Metal plates with cutting edges were close to the undersides of the beams on every side of the notch. This arrangement enabled the size of the "crack mouth opening displacement (CMOD)" using a clip gauge (Figure 8a). Table 1 summarizes the results of four separate measurements taken of the fracture width. At a displacement rate of 0.01mm/min, all beams were bent three-points under CMOD control (Figure 8b). As shown in Figure 3.8, step A of Table 1, loading was stopped as soon as the macro-crack reached the target CMOD of 0.3 mm. After then, the beams were released.

Table 1: Stages for measuring crack opening

	Stage	**Measurement device**
A	Target CMOD (0.3mm)	Clip gauge
B	At complete unloading	Clip gauge
C	Unloading, after 24h rest	Microscope
D	12h after thermal activation	Microscope

Figure 8: (a) The beam with thin metal bars attached (b) the 3-point bending test apparatus with the CMOD clip gauge connected

2.4 Evaluations using microscopy and activation of k-SMP

Once the samples were unloaded, they were laid flat for a day prior to thermal activation. Stages C and D of the thermal activation process were monitored by measuring the crack width consuming an optical microscope and a 10x Moticam camera. Both the front (X-side) and back (Y-side) of each beam had its crack-widths measured at two separate locations, as shown in Figure 9.

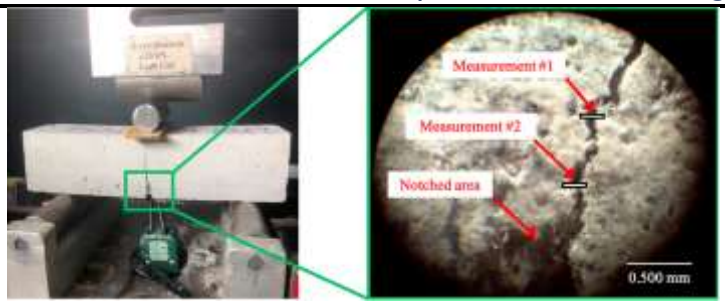

Figure 9: Specifics of the crack width measurements made under the microscope

3. Result and Discussion

Pre- and post-thermal activation crack width measurements were taken for the k-SMP fibers. All AD and RD specimens showed a decrease in crack widths at every single measurement point after thermal activation. The crack width dimensions for the AD series (6 specimens) are shown in Figure 10a for side X and side Y, correspondingly. The dimensions were taken before and after thermal activation, at sites #1 and #2, according to stages C and D in Table 1. Figure 10a shows that after thermal activation, the fracture width was measured to be among 0 and 0.025 mm, with a mean of 0.010 mm and a standard deviation of 0.007 mm.

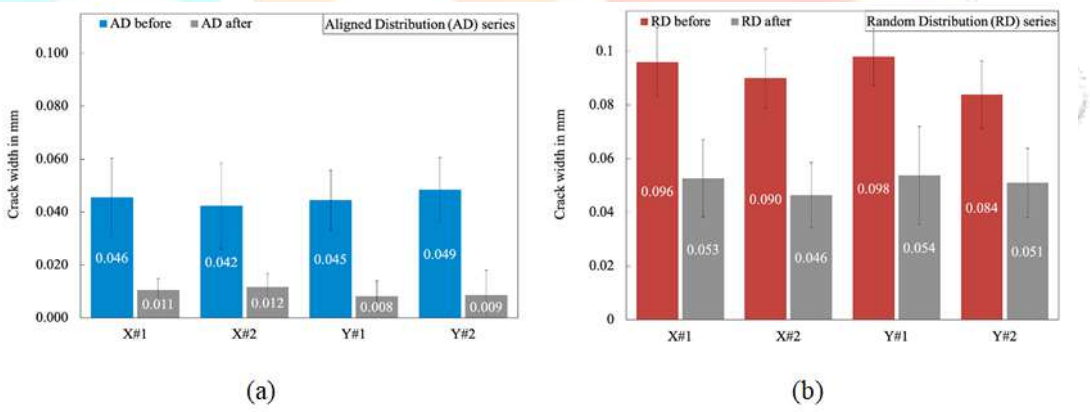

Figure 10: The average crack widths of the samples in the AD series and the RD series

Figure 11a shows the average fracture closure levels, with certain samples (such as AD2, AD3, and AD5) showing complete closure. The standard deviation was 16%.

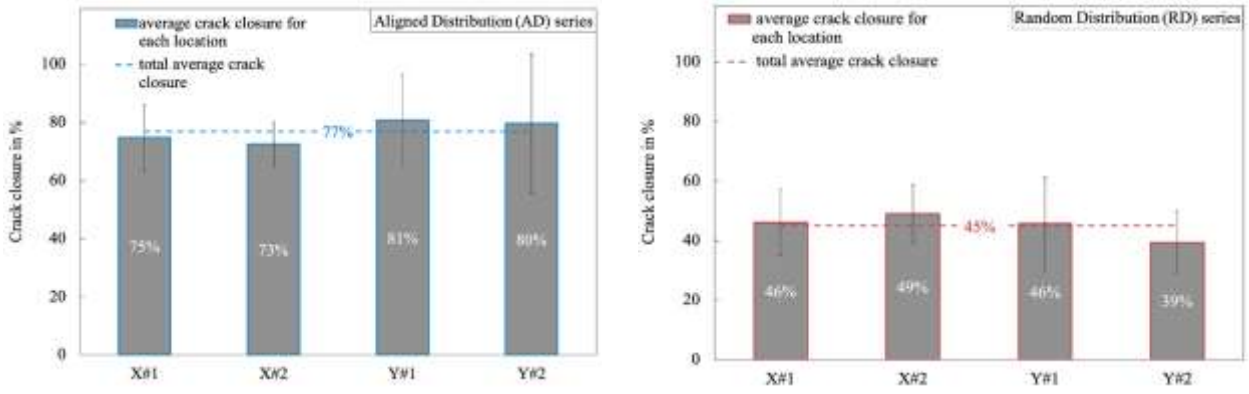

Figure 11: Average values for fracture closure on the X and Y axes, and in the two locations of (a) AD series and (b) RD series samples

Figure 12a and Figure 12b show example microscope pictures of the crack aperture before and after heat activation, respectively, for sample AD3.

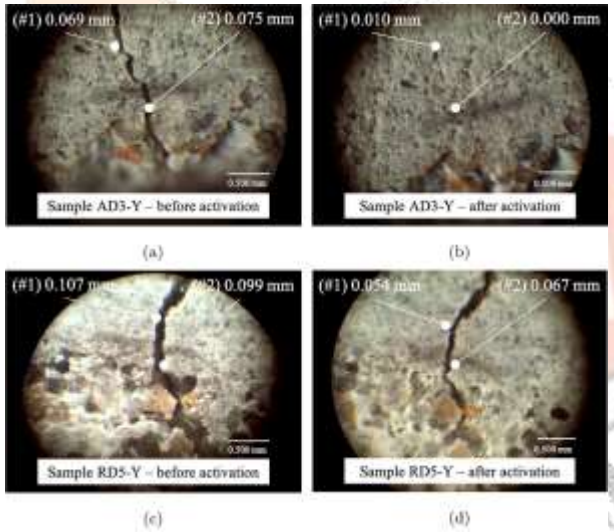

Figure 12: Examining the AD3 sample under a microscope to see the fracture width measurements

Figure 10b shows that the bigger specimens with random fibers consistently displayed a crack opening on the X-side and Y-side of the beams prior to heat activation. The crack widths measured after thermal activation ranged from 0.025 to 0.075 mm, and almost 45%, as appreciated in Figure 11b. Figure 12c shows the fracture in the RD beam before thermal activation and Figure 12d displays the crack after thermal activation for sample RD5, Y-side. Figure 13 show that both the AD and RD series had residual fracture widths after activation that is less than 150μm. This is a threshold below which the possibility of auto-genous repair is significantly enhanced.

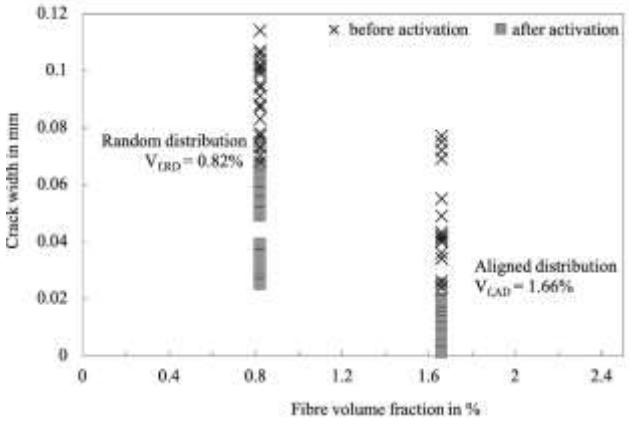

Figure 13: Pre- and post-heat-activation crack widths for the RD and AD series

To get a better understanding of the fibers in the volume around the fracture, this research additionally acquired X-CT images (notched region). The X-Ray photos shown here were captured with a 9 µ m pixel size resolution, an accelerating voltage of 100 kV, and an exposure time of 2736ms. Figure 14 shows the 3D reconstruction.

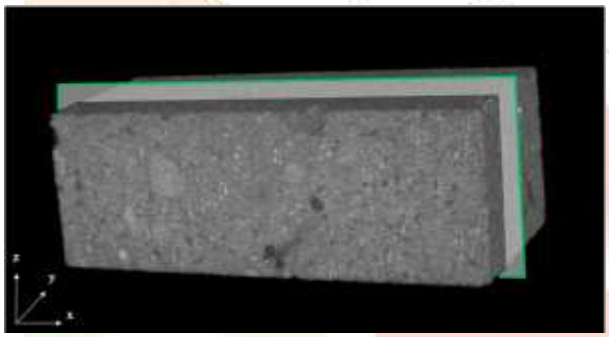

Figure 14: 3D reconstruction of a section of sample RD4

The k-SMP fiber implanted in the mortar could be seen in a cross-sectional view on the y-axis ("Figure 14, green plane, and Figure 15a"). After being thermally activated, a k-SMP filament bridges a macro-crack in Figure 15b), which displays an enlarged section of 30 × 30 mm.

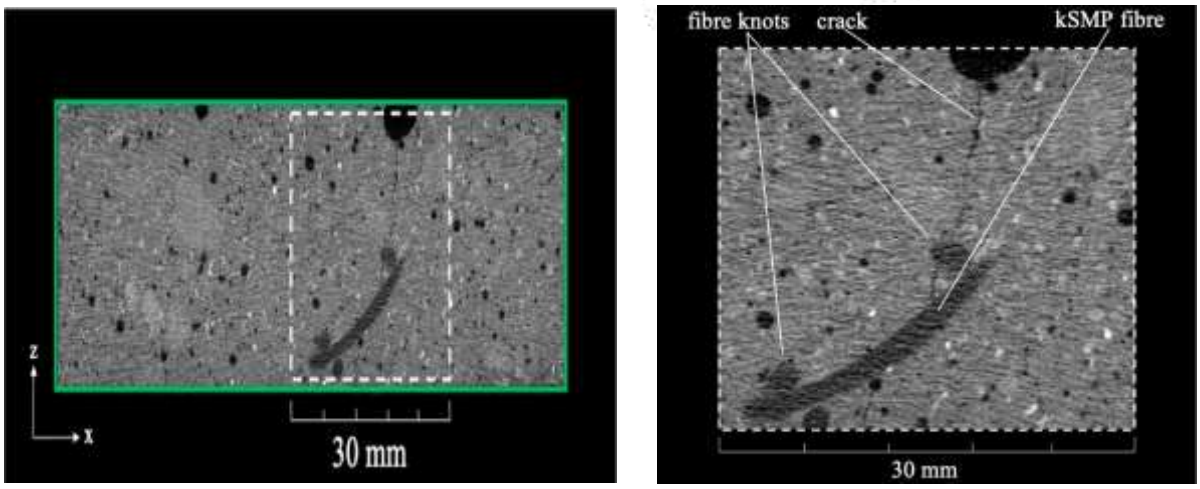

Figure 15: The X- CT scan of (a) the thermally activated RD4 sample and (b) a magnified view revealing the k-SMP fiber and crack

4. Conclusion

The main objective of the study was to develop and test crack-closing capacity of MRCC supported k-SMP in fibers which are specifically designed based in the road constructions. The procedure was to include PET-based k-SMP fibers in mortar specimens in two possible ways, i.e., with AD and RD. The experimentation procedure involved preparation of conventional mortar mixtures; casting of fiber reinforced elements as well as controlled notching to create cracks. The tests were done under CMOD control where the tests were simulated to crack followed by elevating the samples to 150oC to induce fiber shrinkage and close the cracks. The findings exhibited encouraging results to self-healing performance:

- In AD specimens, an average crack closure of 77% was achieved, with several specimens exhibiting complete crack closure.
- RD specimens showed a notable 45% average crack reduction after thermal activation.
- X-CT imaging confirmed effective fiber bridging, favorable alignment in AD specimens, and strong mechanical anchoring provided by knotted fiber ends.

Reference

1. Han, Chengjia, Tao Ma, Ju Huyan, Xiaoming Huang, and Yanning Zhang. "CrackW-Net: A novel pavement crack image segmentation convolutional neural network." IEEE Transactions on Intelligent Transportation Systems 23, no. 11 (2021): 22135-22144.
2. Munawar, Hafiz Suliman, Ahmed WA Hammad, Assed Haddad, Carlos Alberto Pereira Soares, and S. Travis Waller. "Image-based crack detection methods: A review." Infrastructures 6, no. 8 (2021): 115.
3. Amhaz, Rabih, Sylvie Chambon, Jérôme Idier, and Vincent Baltazart. "Automatic crack detection on two-dimensional pavement images: An algorithm based on minimal path selection." IEEE Transactions on Intelligent Transportation Systems 17, no. 10 (2016): 2718-2729.
4. Oliveira, Henrique, and Paulo Lobato Correia. "Automatic road crack detection and characterization." IEEE Transactions on Intelligent Transportation Systems 14, no. 1 (2012): 155-168.
5. Yuan, Qi, Yufeng Shi, and Mingyue Li. "A review of computer vision-based crack detection methods in civil infrastructure: Progress and challenges." Remote Sensing 16, no. 16 (2024): 2910.
6. Tabaković, Amir, and Erik Schlangen. "Self-healing technology for asphalt pavements." Self-healing materials (2016): 285-306.
7. Ahn, Tae-Ho, and Toshiharu Kishi. "Crack self-healing behavior of cementitious composites incorporating various mineral admixtures." Journal of Advanced Concrete Technology 8, no. 2 (2010): 171-186.

8. Xue, Caihong, Wengui Li, Fulin Qu, Zhihui Sun, and Surendra P. Shah. "Self-healing efficiency and crack closure of smart cementitious composite with crystalline admixture and structural polyurethane." Construction and Building Materials 260 (2020): 119955.

9. Lu, Qi, Kisuk Choi, Jae-Do Nam, and Hyoung Jin Choi. "Magnetic polymer composite particles: Design and magnetorheology." Polymers 13, no. 4 (2021): 512.

10. Thevenot, Julie, Hugo Oliveira, Olivier Sandre, and Sébastien Lecommandoux. "Magnetic responsive polymer composite materials." Chemical Society Reviews 42, no. 17 (2013): 7099-7116.

11. Styer, Jaime, Lori Tunstall, Amy Landis, and James Grenfell. "Innovations in pavement design and engineering: A 2023 sustainability review." Heliyon 10, no. 13 (2024).

12. Khawaja, Hassan, and Ahmad Tanveer. "Review of low-temperature crack (LTC) developments in asphalt pavements." (2018).

13. Srinivasa, C. H., and Dr Venkatesh. "A literature review on engineered cementitious composites for structural applications." International Journal of Engineering Research and Technology 3, no. 12 (2014): 531-537.

14. Huang, Silu, Qiuni Fu, Libo Yan, and Bohumil Kasal. "Characterization of interfacial properties between fibre and polymer matrix in composite materials–A critical review." Journal of Materials Research and Technology 13 (2021): 1441-1484.

15. Fang, Chaolin, and Varenyam Achal. "Enhancing engineering properties of cement mortars through microbial self-healing and community analysis." Construction and Building Materials 462 (2025): 139934.

16. Han, Qiangqiang, Lu Jiang, Yu Zhang, Wenjing Wang, Pengjun Li, Wei Lu, Hua Xia, and Zhu Li. "Study on crack-healing effect of cement mortar with fiber under dynamic water environment." Journal of Building Engineering 72 (2023): 106567.

17. Teall, Oliver, Martins Pilegis, John Sweeney, Tim Gough, Glen Thompson, Anthony Jefferson, Robert Lark, and Diane Gardner. "Development of high shrinkage polyethylene terephthalate (PET) shape memory polymer tendons for concrete crack closure." Smart Materials and Structures 26, no. 4 (2017): 045006.